Interaction of Potential Vorticity Anomalies in Extratropical Cyclogenesis. Part I: Static Piecewise Inversion

ZONGHUI HUO

CMRP, School of Meteorology, University of Oklahoma, Norman, Oklahoma

DA-LIN ZHANG

Department of Meteorology, University of Maryland, College Park, Maryland

JOHN R. GYAKUM

Department of Atmospheric and Oceanic Sciences, McGill University, Montreal, Quebec, Canada

ABSTRACT

The relative importance of various potential vorticity (PV) perturbations and their mutual interactions associated with the superstorm of 12–14 March 1993 are investigated by applying a piecewise PV inversion diagnostic system to a 36-h simulation of the storm. It is shown that the contributions from all PV anomalies to the surface development increase with time, although their relative significance varies during the rapid deepening stage. In general, the upper-level dry PV anomalies contribute the most to the rapid deepening of the storm, followed, in order, by the lower-level thermal anomaly and latent heat release.

Comparing the PV anomalies and their inverted circulations reveals that there exists a favorable phase tilt between the upper- and lower-level anomalies that allows lower- and upper-level mutual interactions, in which the circulations associated with the upper-level PV anomalies enhance the lower-level anomalies and vice versa. In addition to the vertical interactions, lateral interactions are also present among the upper-level PV anomalies and the background flow. It is also found that the background flow advection dominates the vortex–vortex and vortex–background flow interactions in the deepening of the storm. The vortex–vortex interactions of the two upper-level positive PV anomalies cause the negative tilt of the main upper-level trough during the rapid deepening period.

1. Introduction

Since the seminal work of Hoskins et al. (1985), a growing number of studies have used the potential vorticity (PV) concept to gain a better understanding of extratropical cyclones and the interactions among different processes or entities leading to cyclogenesis. Indeed, the PV concept provides an alternative approach to envisaging the influence of upper-level PV anomalies on the downstream development of a surface cyclone (Boyle and Bosart 1986; Uccellini et al. 1987; Whitaker et al. 1988; Bleck 1990; Reed et al. 1992), in contrast to the conventional synoptic thinking of upper-level troughs influencing surface cyclones (Petterssen 1956; Sanders 1986, 1988).

The PV concept is especially attractive to use because

of (a) its conservative property in the absence of diabatic heating and friction, and (b) its invertibility principle; that is, a knowledge of the PV distribution and boundary potential temperature is sufficient to infer the meteorological fields (e.g., winds, temperatures, and geopotential heights) subject to some balanced flow constraints. Numerous studies have used various piecewise PV inversion schemes to examine the dynamical effects of upper- and lower-level PV anomalies on surface cyclogenesis (e.g., Davis and Emanuel 1991; Black and Dole 1993; Davis et al. 1993; Hakim et al. 1996). For example, Davis and Emanuel (1991) proposed a piecewise PV inversion technique to isolate the relative contributions of upper- and lower-level PV anomalies to surface cyclogenesis. The same technique was later utilized to examine the importance of initial structures and diabatic heating in an observed cyclogenesis event (Davis 1992), and the integral effect of condensational heating in a simulated winter storm (Davis et al. 1993). These studies indicate that (i) the piecewise PV inversion technique is a useful tool to diagnose the interac-

Corresponding author address: Dr. Da-Lin Zhang, Department of Meteorology, Room 3433, Computer and Space Science Building, University of Maryland, College Park, MD 20742-2425.
E-mail: dalin@atmos.umd.edu

tions between different PV anomalies in a cyclone system, (ii) the presence of an upper-level PV anomaly and its position relative to surface disturbances are both critical, and (iii) the primary effect of condensation is simply to superpose a positive PV anomaly onto a baroclinic circulation and the cyclogenesis is basically driven by baroclinicity in nature. Recently, Hakim et al. (1996) utilized a piecewise quasigeostrophic PV (QGPV) inversion scheme to study the lateral interactions between two upper-level PV anomalies and background flow in a trough-merger cyclogenesis case. They identified and quantified three types of interactions: vortex–vortex, advection of background QGPV by vortex-induced flows, and advection of vortex QGPV by background flows. They found that the rapid cyclogenesis occurs as the two upper-level vortices achieve their closest proximity. With a piecewise PV tendency diagnosis, Nielsen-Gammon and Lefevre (1996) examined the contributions of different processes to the development of an upper-level mobile trough. Their approach differs from the previous ones in that only instantaneous effects could be evaluated.

The PV inversion techniques have also been applied to the improvement of model initial conditions in simulating extratropical cyclones. For instance, Huo et al. (1998) used the piecewise PV inversion developed by Davis and Emanuel (1991) to include the influence of observed surface temperatures over the Gulf of Mexico into the model boundary layer by treating it as a surface PV surrogate. With the improved initial conditions, they obtained a simulation of the 12–14 March 1993 superstorm, also referred to as "the storm of the century," that is superior to the simulation without the corrected boundary layer in terms of both the track and intensity.

The purpose of this study is to provide a better understanding of the interaction of upper-level PV anomalies in the development of the 12–14 March 1993 superstorm using the more realistic simulation as presented in Huo et al. (1998). Specifically, Huo et al. (1995), Kocin et al. (1995), and Uccellini et al. (1995) have shown that intense low-level baroclinicity and upper-level jet streaks, strong surface fluxes from the ocean, the merging of two upper-level short-wave troughs or PV anomalies, and intense diabatic heating all contributed to the rapid deepening of the superstorm. However, uncertainty still remains concerning the relative importance of these processes as well as their interactions in the rapid cyclogenesis. In particular, what are the roles of the two troughs? How do they interact with the surface processes in intensifying the storm? Thus, the objectives of this study are to (i) gain insight into the vertical and lateral interactions of various major PV anomalies during the development of the storm, and (ii) quantify the effects of different dynamical and physical processes on the surface cyclogenesis using the piecewise PV inversion technique developed by Davis and Emanuel (1991). This diagnostic system is based on the invertibility principle of PV, which supports a

dynamic partition of the total PV field into many significant portions. The circulation associated with each portion of the PV field can be deduced individually. In principle, such an approach provides a means to (i) calculate the contributions of selected PV perturbations to the instantaneous cyclone intensity, and (ii) quantify the dynamical interactions between discrete PV features in the flow field and their influences on the flow's subsequent evolution. The results so obtained will provide useful background information for Part II of this series of papers (Huo et al. 1999) in which the impacts of the two troughs and their interactions with diabatic heating and large-scale baroclinicity on the surface cyclogenesis will be examined by treating their associated PV anomalies as an initial-value problem.

The next section provides a brief overview of the structures and evolution of PV associated with the storm during its rapid cyclogenesis stage from the 36-h model simulation given in Huo et al. (1998). Section 3 contains a brief summary of the piecewise PV inversion system and the procedures used for the present case study. Section 4 presents the analysis of the contributions of various PV anomalies to the cyclone's intensification. Section 5 shows the dynamical interactions between upper- and lower-level PV anomalies, whereas section 6 examines the lateral interactions between the upper-level PV anomalies. A summary and concluding remarks are given in the final section.

2. Structures and evolution

For the convenience of subsequent discussions, we review briefly the PV structures of the superstorm; see Huo et al. (1995) for more details. At 0000 UTC 13 March (i.e., 12 h into the integration), hereforth 13/00–12, there are two distinct features of PV at 400 hPa: a northern tongue of large PV (>3.5 PVU, 1 PVU $= 10^{-6}$ m² K s⁻¹ kg⁻¹) over the central United States and a southern PV maximum over the western Gulf of Mexico (Fig. 1a). The northern (southern) PV tongue corresponds approximately to a northern (southern) upper-level trough (see Fig. 2c in Huo et al. 1995). An examination of the vertical cross section (Fig. 1d) shows that the two PV maxima result from the descent of a dry stratospheric high-PV reservoir, which is further evidenced by the model-generated cloud-free region associated with the PV tongue and nearly saturated conditions to its east (Fig. 1a). The intensification of the two midlevel troughs is a consequence of continued descent of the stratospheric dry and warm air (Fig. 1d). The flow vectors in the vicinity of the storm suggest that the PV at the tip of the southern depression is being advected toward the cyclone center by southwesterly currents. This advection of high PV would increase the cyclonic vorticity of the storm (Hoskins et al. 1985) and provide an important forcing for the rapid cyclogenesis in the prior 12 h when the cyclone travels from the northwestern Gulf of Mexico to the south of the Mis-

sissippi River delta. At 850 hPa, an elongated zone of PV is distributed downstream of the upper-level PV anomaly with a maximum value exceeding 1 PVU located to the northwest of the cyclone center. Most of this lower-level PV concentration is created by an upward increase in latent heat release in cloud regions. In the upper levels above the layers of latent heat release, however, heating destroys PV and creates the tight PV gradient around the outskirts of the "comma shaped" cloudiness. Note that the lower- and upper-level PV anomalies are in a favorable phase for cyclonic development. The lower-level broad baroclinic zone (see Fig. 1 in Huo et al. 1995), which occurred 12 h earlier (i.e., at 12/12–00), also experiences rapid changes, namely, strong cold (warm) advection behind (ahead of) the surface cold fronts begins to generate a large cold (warm) anomaly (Fig. 2a).

By 13/12–24, the southern PV anomaly has moved to the western Florida peninsula, and begun to experience the influence of southwesterly flows with weak upward motion (Fig. 1b). Subsequently, the southern PV anomaly weakens with time while being advected toward the surface cyclone center. The northern PV anomaly to the west, on the other hand, has moved rapidly into the base of the short-wave trough, enhancing its associated cyclonic circulations. The two PV anomalies merge into one strip 6 h later and only a single short-wave trough becomes evident (not shown). By comparison, the lower-level PV anomaly, intensifying with time, expands along the warm front near the cyclone center with increased overlap with its upper-level counterpart. Similarly, the low-level thermal wave continues to amplify as a result of advection, causing marked increases of the thermal gradient near the triple point of the cold/warm fronts (Fig. 2b).

At 14/00–36, the upper-level PV ribbon has wrapped around the short-wave trough (Fig. 1c). The surface cyclone is being overtaken by the leading portion of the merged PV ribbon; so this time marks the end of the storm's explosively deepening phase. The vertical cross section of PV taken through the cyclone center shows two distinctive PV concentrations in the vertical: one is the merged PV anomalies at upper levels in the cloudless dry air, and the other is the diabatically produced PV anomaly centered in the 900–800-hPa layer within the cloudy air. Descending motion prevails within the upper-level dry PV region except to its northern edge where upward motion occurs as a result of latent heat release along the warm front. We can see that the dry stratospheric large-PV air, denoted by the 1-PVU contour,
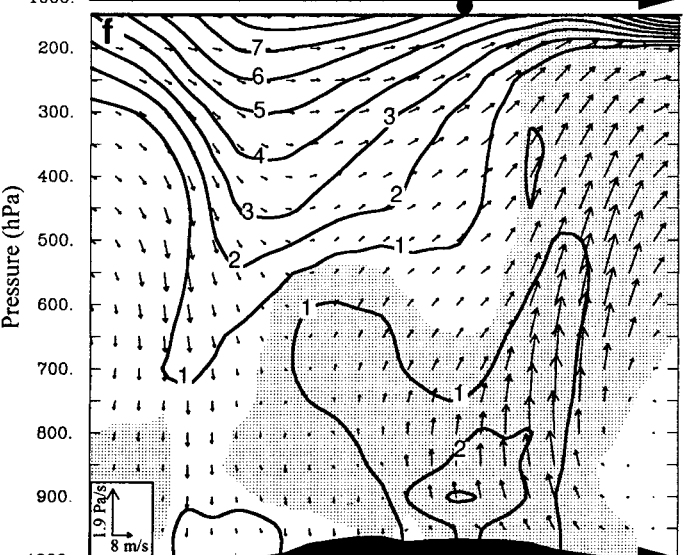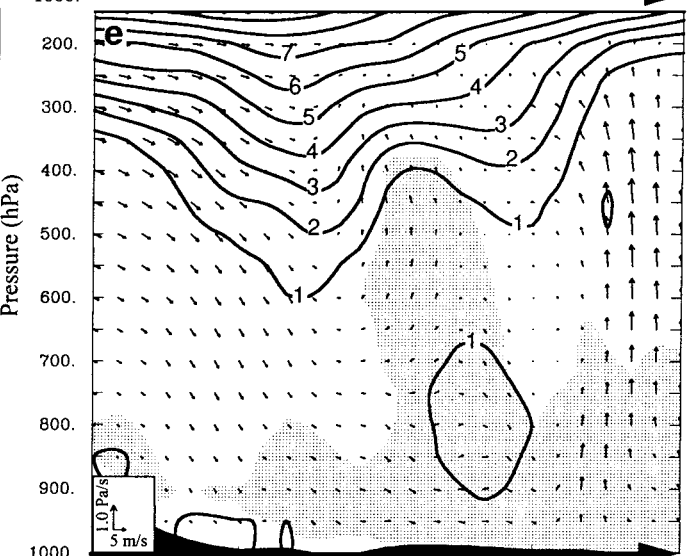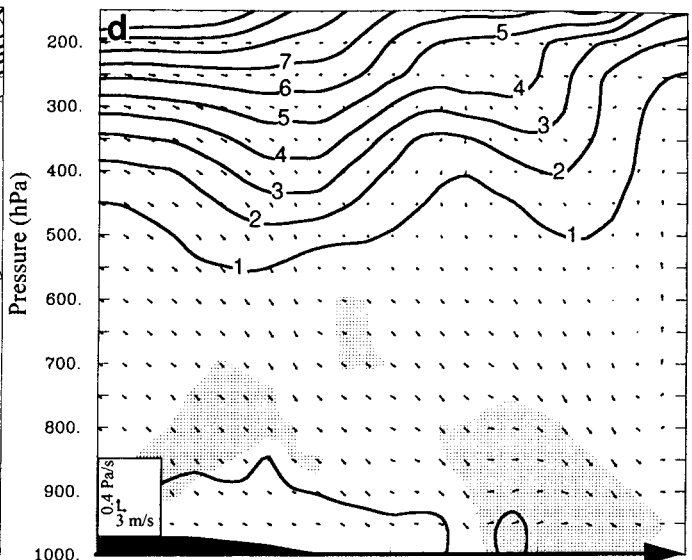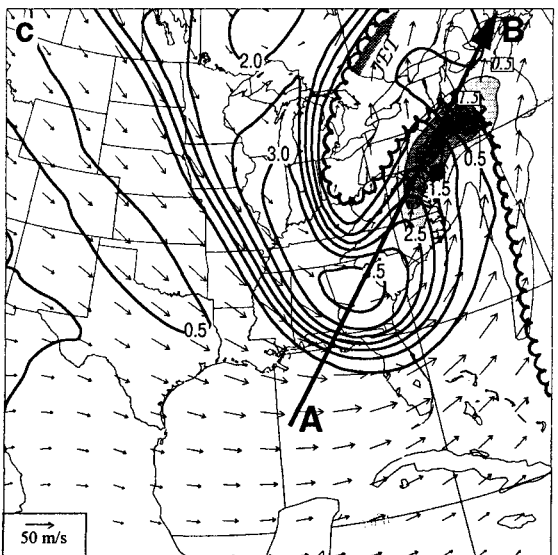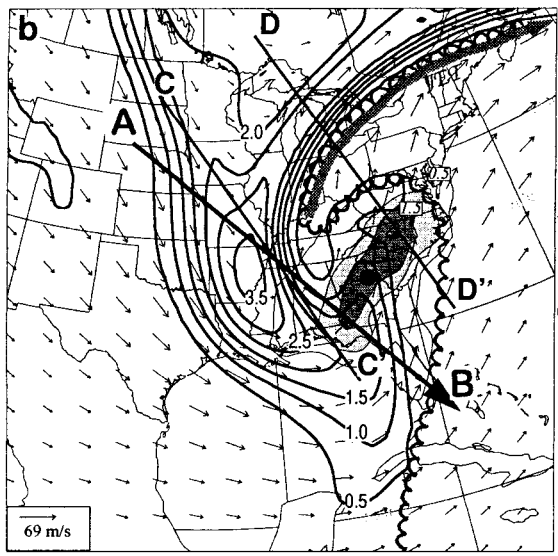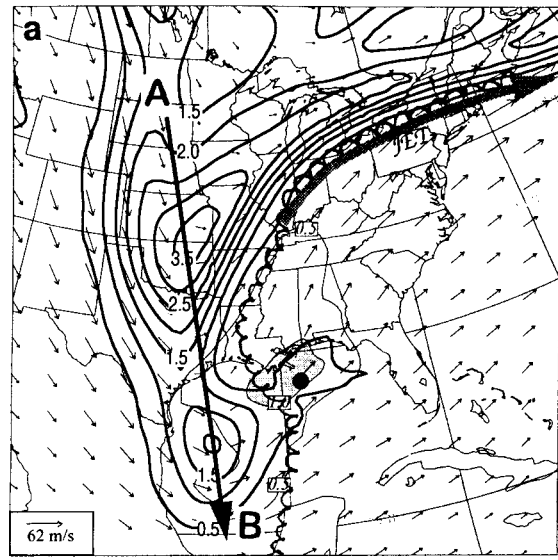
penetrates downward as low as 700 hPa not far behind the cyclone center. The descending tropopause large-PV air above the surface low implies that the cyclonic circulation induced by the PV anomaly may have assisted the surface cyclone development. In the following sections, we will use a piecewise PV inversion diagnostic system as developed by Davis and Emanuel (1991) to quantitatively assess the interactions between the upper- and lower-level PV anomalies and their importance in the surface cyclogenesis.
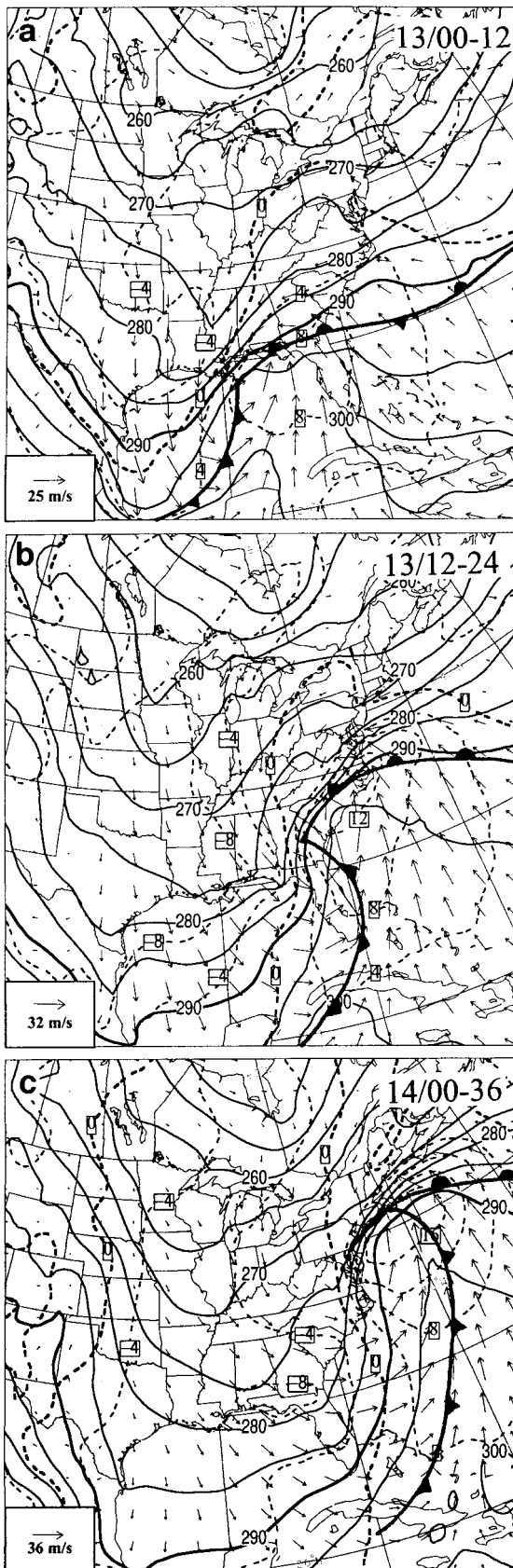
3. Isolating PV anomalies

In this section, we describe procedures on how to compute balanced flows associated with each of the above-mentioned anomalies. First, we need to define a mean state to isolate each PV perturbation. The mean state for the present case is defined as the time average between 0000 UTC 11 March and 0000 UTC 15 March 1993, which approximately corresponds to one synoptic-scale wave period. Given the mean state, the total PV anomaly is computed simply as the departure from the time average.

The next step is to partition the total PV anomaly field in a dynamically meaningful way. The philosophy of partitioning the total PV perturbations is to isolate distinct perturbations of different origins and to examine their interactions with each other and with the mean PV. In the present case, these are perturbations from the tropopause depression, the surface baroclinicity, and the interior troposphere that is associated with latent heat release. It is evident from Figs. 1 and 2 that the stratosphere-related PV perturbations (Q_d) could be defined as positive PV anomalies lying in the dry air with relative humidity less than 30%, which includes the upper boundary and positive dry anomalous PV from 200 to 800 hPa, mainly of stratospheric origin. The lower-tropospheric PV perturbations associated with condensational heating (Q_h) are defined as positive PV anomalies with greater than 70% relative humidity and in layers below 500 hPa. The subsaturated threshold value of 70% relative humidity is chosen to include PV that may be advected out of the precipitation region. The surface potential temperature perturbation can also be regarded as equivalent to a concentrated PV anomaly contained in a thin surface layer. Because of the surface heat flux, the lower-level interior PV is strongly influenced by the boundary layer, and the circulation associated with the lower-level PV anomaly opposes that at the surface. Therefore, we will follow the procedure of Davis (1992)

→

FIG. 1. (left panels) The distribution of 400- (solid) and 850-hPa (shading) PV at intervals of 0.5 PVU, superposed with 400-hPa wind vectors at (a) 13/00–12, (b) 13/12–24, and (c) 14/00–36. (right panels) Vertical cross sections of PV, superposed with along-plane flow vectors, which are taken along lines given in corresponding figures in the left panels. Shading on the right panels and the scalloping on the left panels show the distribution of cloudiness determined by relative humidity higher than 80%. Thick shaded arrow denotes upper-level jet streak and solid circle denotes the cyclone center.

and group the lower boundary and the lower-level interior PV at 900 hPa (except where the lower-level PV anomaly coincides with larger than 70% relative humidity), forming the effective lower boundary (θ_{eff}). Finally, the remainder of the interior PV perturbations, consisting of primarily the negative PV perturbation associated with the upper-level waves, will be referred to as Q_r.

The piecewise PV inversion technique of Davis and Emanuel (1991) is used to perform three-dimensional inversions of Q_d, Q_h, Q_r, and θ_{eff}, using a standard successive overrelaxation technique. The inverted winds, temperature, and height fields will help reveal how the different PV anomalies interact and what their relative contributions are to the surface cyclogenesis. When inverting each anomaly, we set the other anomalies equal to zero, assuming homogeneous lateral boundary conditions. The PV inversion is performed every 6 h from 1200 UTC 12 March to 0000 UTC 14 March.

4. Cyclogenesis attributions

Table 1 shows the area-averaged contributions from the aforementioned four PV elements to the 1000-hPa height perturbation at the cyclone center during the whole period of cyclogenesis. It is evident that the magnitudes of all the contributions increase with time, an indication of the cyclone's intensification. The relative contribution of diabatic heating Q_h (18%–24%) is the smallest and does not change much during the deepening period. However, those of Q_d and θ_{eff} behave differently during the different stages of the cyclogenesis. For example, the relative contributions of Q_d and θ_{eff} between 12/12–00 and 13/00–12 are about 38%–40%. After 13/00–12, the Q_d contribution grows faster than that of θ_{eff} owing to the approaching and subsequent merging of the northern PV anomaly into the southern one. Consequently, Q_d becomes the dominant factor in determining the cyclogenesis during the second half of its life cycle, that is, >50%. The different behaviors between Q_d and θ_{eff} occur because after entering the occlusion stage the surface cyclone center is usually located away from the warm sector (cf. Figs. 2b,c) and the Q_d begins to overtake the surface cyclone center. As mentioned in the previous section, Q_r is mainly made up of the negative PV anomaly associated with the mid-to upper-level ridge. Its negative contribution to the cyclone's depth opposes the positive contributions from Q_d, Q_h, and θ_{eff}. The increase of Q_r can be seen as part of the upper-level wave amplification and is strongly

←

FIG. 2. Evolution of 900-hPa potential temperature (solid, every 5 K) and its perturbations (dashed, every 4 K), superposed with 900-hPa wind vectors for (a) 0000 UTC, (b) 1200 UTC 13 Mar, and (c) 0000 UTC 14 Mar 1993.

TABLE 1. The magnitudes (dam) and the relative contributions (%) to the 1000-hPa height perturbation as inverted from the upper-level dry PV anomaly (Q_d), lower-level moist PV anomaly (Q_h), effective bottom boundary (θ_{eff}), and the remaining PV component (Q_r). They are averaged over an area of 300×300 km^2 at the cyclone center.

Day/h	Q_d (dam)	%	Q_h (dam)	%	θ_{eff} (dam)	%	Q_r (dam)	Total
12/12	−11.0	(40.1)	−6.0	(21.9)	−10.4	(37.9)	10.9	−15.5
12/18	−12.2	(37.2)	−6.3	(19.2)	−14.3	(43.6)	15.2	−17.6
13/00	−19.1	(39.7)	−10.3	(21.4)	−18.7	(38.9)	25.1	−23.0
13/06	−27.8	(47.0)	−13.4	(22.6)	−18.0	(30.4)	31.5	−27.7
13/12	−39.0	(52.1)	−16.4	(21.9)	−19.4	(25.9)	41.7	−33.1
13/18	−47.3	(52.5)	−16.7	(18.5)	−26.1	(29.0)	52.7	−37.4
14/00	−53.4	(53.0)	−19.2	(19.1)	−28.1	(27.9)	60.3	−40.4

aided by the increase of Q_h and θ_{eff} through interactive processes that are to be discussed later in the paper.

In order to gain further insight into the results of static PV inversions, Fig. 3 presents the contributions to the cyclone's 6-hourly deepening rates from the above four different PV anomalies. By comparing all the traces, one can see that the contribution from Q_d (Fig. 3b) dominates the cyclone's deepening rates. While the direct contribution from Q_h (Fig. 3c) is small throughout the genesis period, its impact on the storm development is by no means less important than the other contributions. In fact, a sensitivity run, in which the latent heat release is turned off (not shown), shows that all the anomalies become much weaker, indicating the important positive feedback processes of diabatic heating in the cyclogenesis. The net contribution shows that after the initial spinup, the cyclone deepens almost linearly with time (Fig. 3a).

Figure 4 shows the vertical cross section of the balanced height inverted from the aforementioned four PV elements at the mature stage, that is, 14/00–36. The upper-level Q_d induces a deep negative height perturbation throughout the troposphere, with the peak intensity occurring at 400 hPa where the PV anomaly is maximized (Fig. 4a). The Q_d-induced perturbation also expands both upstream and downstream of the upper-level dry PV maximum; it still maintains a slightly upstream tilt with respect to the surface cyclone although the tilt is not as pronounced as before. Its continued influence on the surface cyclogenesis is reflected by the ensuing deepening in the following 6 h until 0600 UTC 14 March (Huo et al. 1995) when the upper-level PV anomaly and the surface cyclone center become more vertically coherent. Similarly, the influence of the Q_r-induced positive height perturbation is also widespread; the largest contribution is associated with the negative PV anomaly near the upper-level ridge (Fig. 4b). However, the Q_r-induced perturbation center, corresponding to the largest negative PV anomaly, never coincides with the surface low during the genesis stage because it develops in the top portion of the ascending flow and downstream of the surface cyclone center. Thus, the negative contribution to the surface cyclogenesis would not possibly dominate, even during the filling stage.

Again, the Q_h-induced height perturbation (Fig. 4c)

is much less pronounced in both intensity and volume coverage than that of the Q_d-induced one. However, its positive contribution to the depth of the surface cyclone is obvious since its maximum perturbation is located in the lower troposphere near the surface cyclone center. The θ_{eff}-induced height perturbation exhibits a positive–negative couplet, which corresponds to the cold–warm air masses in the cyclone's cold–warm sectors (cf. Figs. 4d and 2c). Since the cyclone center is located on the warm side of the θ_{eff} anomaly and since the warm θ_{eff} anomaly is more significant than the cold θ_{eff} anomaly behind the surface cyclone center, the θ_{eff} contribution to the cyclone's depth is positive and increases with time (as shown in both Fig. 2c and Table 1) as a result of increased warm advection into the central region of the storm. Table 1 shows that both Q_h and θ_{eff} contributions increase by almost a factor of 3 during the cyclone development. Furthermore, the Q_h-induced height perturbation is almost in phase with the θ_{eff}-induced one by 14/00–36. Of interest is that the Q_h and θ_{eff} contribute not only to the surface cyclone depth, but also to the upper-level PV anomalies, since their induced height perturbations penetrate into the middle to upper troposphere. This will be discussed in the next section.

It should be mentioned that the above partitioning tends to underestimate the relative (positive) contribution of the effective lower boundary, since θ_{eff} contains not only the surface warm anomaly but also the surface cold anomaly and the lower-level interior PV, as compared to the upper-level contributions (i.e., Q_d and Q_r). Nevertheless, the essence of the piecewise PV inversion is well demonstrated; that is, the contribution from each single PV identity can be quantified.

5. Vertical interactions

We have seen in the preceding section that the piecewise-inverted height and flow fields are in three dimensions and they extend almost into the entire inversion domain. Since these winds are free to interact with other nearby PV elements, both vertical and lateral interactions will occur as the system deepens. In this section, we discuss the possible interactions between the upper- and lower-level PV anomalies and attempt to explain how the interactions could amplify the PV
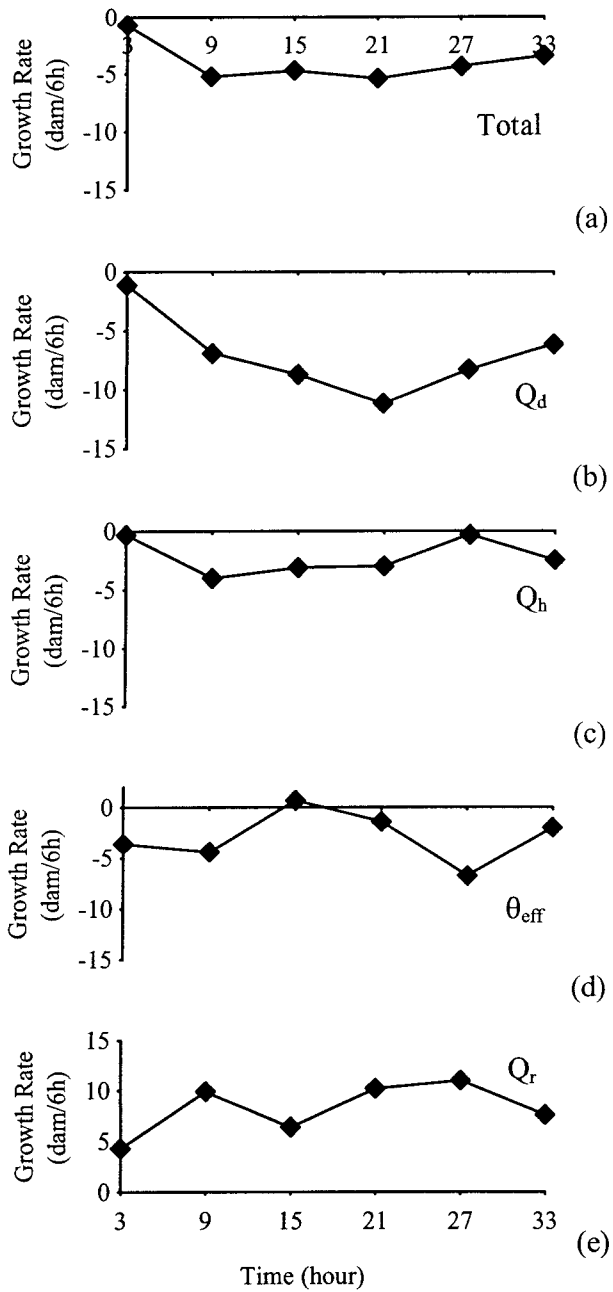
FIG. 3. The contributions to 1000-hPa height change (dam/6 h) from (a) the total PV anomaly (i.e., $Q_d + Q_h + Q_r + \theta_{\text{eff}}$), (b) the upper-level dry PV anomaly Q_d, (c) the lower-level moist PV anomaly Q_h, (d) the effective bottom boundary anomaly θ_{eff}, and (e) the remaining PV anomaly Q_r.
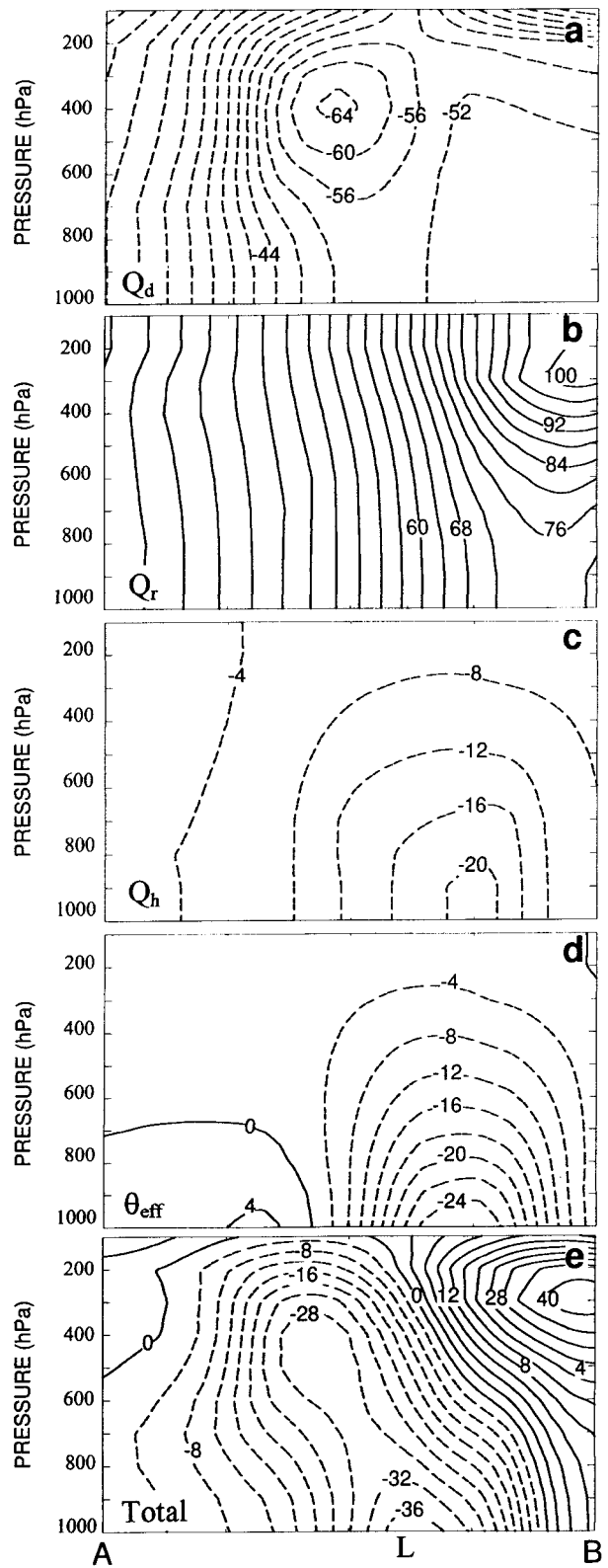
$\rightarrow$

FIG. 4. Vertical cross sections of the balanced geopotential height perturbations, at intervals of 4 dam, inverted from (a) the upper-level dry PV anomaly Q_d, (b) the remaining PV anomaly Q_r, (c) the low-

level moist PV anomaly Q_h, (d) the effective bottom boundary anomaly θ_{eff}, and (e) the total PV anomaly (i.e., $Q_d + Q_h + Q_r + \theta_{\text{eff}}$). Solid (dashed) lines are for positive (negative) values. Cross sections are taken along line AB as given in Fig. 1c.
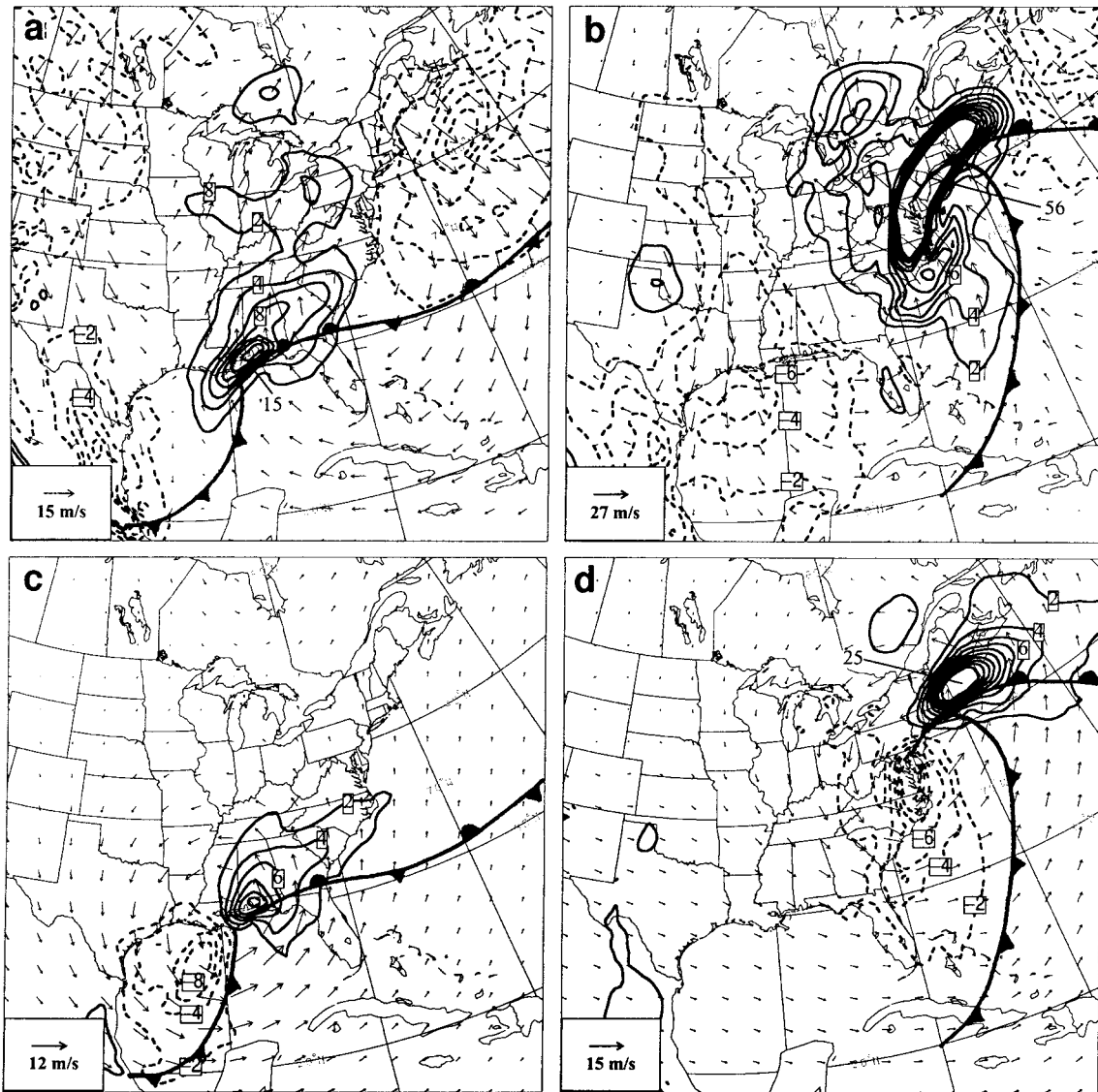
FIG. 5. Potential temperature θ advection (K/6 h) by the balanced flows at 900 hPa that are inverted from (a) and (b) upper-level PV anomalies, i.e., $(Q_d + Q_r)$; (c) and (d) the moist PV anomaly (Q_h). Solid (dashed) lines are for positive (negative) values. Left and right panels are for 0000 UTC 13 Mar and 0000 UTC 14 Mar, respectively.

anomalies. For the convenience of the subsequent discussions, Q_d and Q_r will be combined as upper-level PV anomalies associated with the trough–ridge system while treating Q_h and θ_{eff} as the lower-level PV anomalies. Such a grouping is based on the inverted height perturbations that show clearly two different levels of maximum Lapalacians (see Figs. 4a–d). This methodology is, however, not necessarily unique because they are all closely related. For example, a cold–warm θ_{eff} couplet often implies a strong trough–ridge system in the upper levels, while a high Q_h associated with intense latent heat release may cause the buildup of an upper-level ridge. In the next subsection, we will first examine the influence of the upper-level PV anomaly-induced flows on the lower-level PV anomalies, and then study

how the winds associated with the lower-level anomalies can modify the upper-level anomalies.

a. Influence of upper- on lower-level PV anomalies

As suggested by Reed et al. (1992), the surface thermal anomaly can be treated as a surrogate PV; it is generated mostly by the horizontal advection of the potential temperature θ. Thus, the θ tendencies due to the horizontal advection by 900-hPa winds inverted from the upper-level PV anomalies (i.e., $Q_d + Q_r$ and Q_h) are given in Figs. 5a,b, which show an organized cyclonic–anticyclonic circulation couplet associated with the upper-level trough–ridge system. The induced flow increases in intensity toward the mature stage and its

speed reaches over 25 m s^{-1} by 14/00–36 (Fig. 5b). Since the extent of the surface warmth is determined by both the induced circulations and the thermal gradient, the upper-level trough–ridge system helps build up a warm anomaly in southerly flows, which is maximized in the vicinity of the surface cyclone center (cf. Figs. 2c and 5b). This positive warming tendency is clearly favorable for the spinup of the system, as shown in Fig. 4. In contrast, the development of the cold anomaly in northerly flow is slow and about a half wavelength away from the cyclone center. Thus, the induced cold anomaly by the upper-level trough–ridge system does not contribute significantly to the surface development. The results indicate that upper-level processes leading to *the intensification of low-level southerly flows* tend to have more important effects on the surface cyclogenesis than the northerly or northwesterly flows.

With the induced circulation structures shown in Figs. 5a,b, we can infer a pattern of moisture transport similar to the θ tendencies toward the warm front and cyclone center for latent heat release, which would in turn increase the diabatic generation of lower-level positive PV anomalies (cf. Figs. 1a,b). Since the Q_h anomalies are mainly distributed along the warm front and maximized near the cyclone center, they induce a single cyclonic circulation around the storm with intensity decreasing outward (Figs. 5c,d). The so-induced flows help enhance warm anomalies along the warm front and cold anomalies behind the cold front, thus leading to the amplification of thermal perturbations near the cyclone center. If the thermal tendencies are inverted to the rate of change of height perturbations, the Q_h-induced circulation would contribute little to the deepening rate of the system through the effective boundary. Thus, latent heating tends to have direct effects on the cyclogenesis by warming the midtroposphere and lowering the pressure below.

Finally, the θ_{eff}-induced balance winds, when overlaid on the 900-hPa θ field (not shown), are seen to act to propagate the thermal perturbation downshear along the baroclinic zone, similar to that discussed in Davis (1992). With all the above influences superposed, the low-level thermal wave is deemed to increase, particularly the thermal ridge ahead of the surface low, which itself represents an important part of the surface cyclone development.

b. Influence of lower- on upper-level PV anomalies

Although $Q_d + Q_r$ and $Q_h + \theta_{\text{eff}}$ are different in origin, each contributes to circulations at all levels (see Figs. 4a–d). Thus, the circulations from the lower-level PV anomalies (Q_h and θ_{eff}) must have influences on the development of the upper-level dynamics. To see this point, let us examine the PV advection by the 300-hPa winds induced by Q_h and θ_{eff} (Fig. 6). In general, the induced winds are much smaller in magnitude than the low-level counterpart induced by the upper-level PV

anomalies; the maximum wind is about 5 m s^{-1} (see Fig. 6b). The advection of mean PV by the θ_{eff}-induced winds is mostly positive in the trough and negative over the downstream ridge, acting to amplify the upper-level anomalies throughout the rapid deepening period. Similarly, the winds induced by Q_h also amplify the upper-level positive and negative PV anomalies during the rapid deepening stage (Figs. 6c,d). In addition, increasing Q_h implies rapid latent heat release in the midtroposphere, which assists the amplification of the negative anomaly in the ridge by (i) transporting the upper-level positive PV down to the lower levels, and (ii) creating divergent outflow such that the negative PV anomaly expands in area coverage. It follows that although the upper-level winds induced by the low-level PV anomalies are weak, the development of Q_h and θ_{eff} facilitates the amplification of the upper-level baroclinic wave.

In summary, the favorable phase relationship between the upper- and lower-level disturbances during the rapid deepening stage allows different anomalies to interact constructively with each other. In this regard, cyclogenesis may be viewed as a mutual interaction of the upper- and lower-level PV anomalies, as also discussed by Davis and Emanuel (1991), in which the circulations associated with the upper-level PV anomalies enhance the lower-level anomalies, and vice versa.

6. Lateral interactions

Huo et al. (1995) showed that there are two upper-level PV anomalies or troughs contributing to the surface cyclogenesis. They are separated by more than 3000 km prior to the genesis over the northwestern Gulf of Mexico. They first approach and finally "merge" as the surface cyclone deepens. The scenario fits the description of the trough-merger process by Gaza and Bosart (1990), who performed a climatological study of the trough-merger events in North America. They found that (i) two-thirds of the 21 trough-merger events they examined are associated with explosive cyclogenesis; (ii) the meridional tilt of the principal 500-hPa height trough axis changes from positive to negative prior to the rapid cyclogenesis; and (iii) the two 500-hPa vorticity maxima amalgamate into a single maximum with larger amplitude than either of them. Therefore, it is of interest to examine how these troughs or PV anomalies interact to form the upper-level jet and the surface cyclogenesis.

To study the lateral interactions of the two troughs, we must isolate the related PV anomalies as done in the previous sections. In the present case, they include two positive dry PV anomalies associated with the upper-level troughs (i.e., Q_{d1} for the northern trough and Q_{d2} for the southern trough), and one negative anomaly (R) representing the downstream ridge. The negative PV anomaly (R) is determined by ≤ -0.2 PVU at all levels above 500 hPa. The rest of the PV perturbations (i.e., other than Q_{d1}, Q_{d2}, and R) and the mean PV will be called the background PV—an approach similar to that
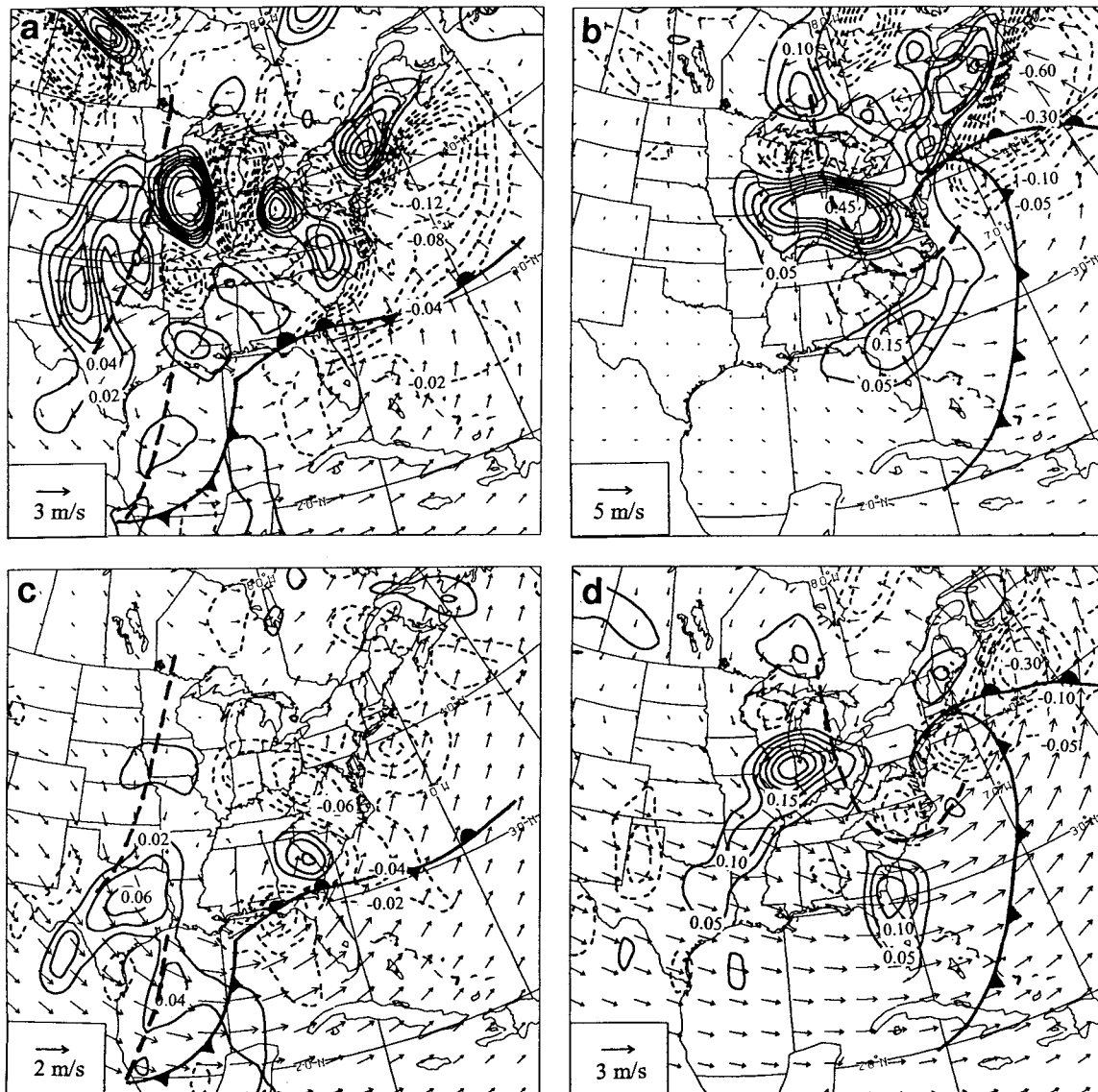
FIG. 6. The PV advection (PVU/6 h) by the balanced flows at 300 hPa that are inverted from (a) and (b) the effective bottom boundary PV anomaly θ_{eff} and (c) and (d) the low-level moist PV anomaly Q_h. Solid (dashed) lines are for positive (negative) values. Left and right panels are for 0000 UTC 13 Mar and 0000 UTC 14 Mar, respectively. Thick-dashed lines denote the upper-level trough axes.

of Hakim et al. (1996). In this way, Q_{d1} and Q_{d2} can be cleanly separated up to 13/06–18.

Following Hakim et al. (1996), we use Fig. 7 to illustrate qualitatively the expected dynamic interactions for the upper-level PV anomalies (Q_{d1}, Q_{d2}, R) and the background flow at 13/00–12. Let us discuss first the vortex–vortex interaction among Q_{d1}, Q_{d2}, and R. Between Q_{d1} and Q_{d2}, there exist advections by their induced circulations and the main contribution of the instantaneous tendencies is cyclonic relative motion of the vortices such that the southern system moves eastward with the background flow, while the northern system moves westward against the background flow (Fig. 7a). The instantaneous tendencies caused by the interactions

of Q_{d1} with R and Q_{d2} with R force a northward motion of all three anomalies (Fig. 7b). In addition to the vortex–vortex interaction, there are also interactions of individual vortices with the background flow. The advections of the background PV by Q_{d1} and Q_{d2} tend to induce instantaneous height falls (rises) west (east) of the vortices and cause the vortices to propagate westward (Fig. 7c). Likewise, the advections of the background PV by R forces a height rise (fall) west (east) of R, and therefore R will move westward against the background flow as well (Fig. 7c). This is essentially the Rossby wave propagation mechanism. Finally, all these vortices are advected eastward by the background flow (Figs. 7d). For the present case, the advection of
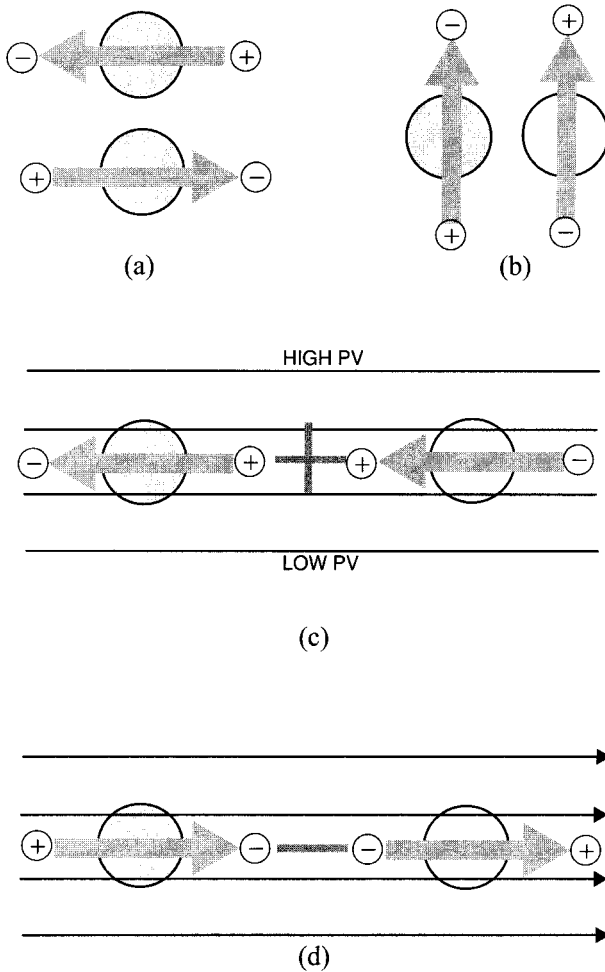
FIG. 7. Schematic illustration of geopotential height tendencies associated with (a) and (b) vortex–vortex interaction, (c) advection of background PV by vortex-induced flows, and (d) advection of PV anomalies by background flows. Shaded and open circles represent positive and negative upper-level PV anomalies, respectively. Positive and negative signs indicate the sense of geopotential height tendencies. Thick arrows show the instantaneous motion of the anomalies and thin arrows show the background flow motion.
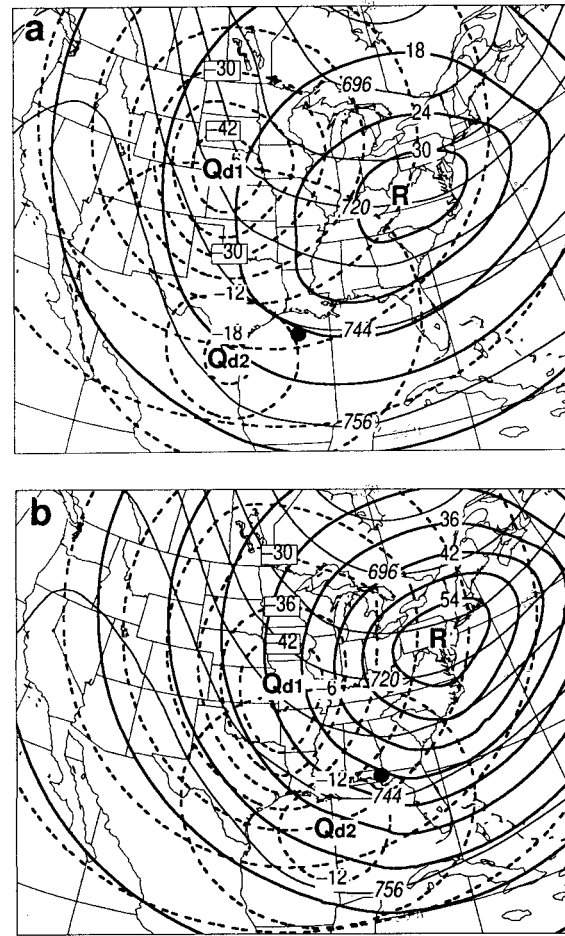

FIG. 8. Inverted 400-hPa balanced geopotential height from the northern PV anomaly (Q_{d1}, dashed), southern PV anomaly (Q_{d2}, dashed), the upper-level negative PV anomaly (R, thick solid), and the background PV (thin solid) at intervals of 6 dam for (a) 1800 UTC 12 Mar and (b) 0600 UTC 13 Mar. Solid circles show the surface cyclone center.

background flow dominates the entire evolution, as implied by the eastward movement of the whole weather system.

Quantitative presentations of the lateral interactions are given in Fig. 8, which shows the significant overlap of the inverted balanced heights associated with Q_{d1}, Q_{d2}, R and background PV at 400 hPa during the intensifying stage (i.e., 12/18–06 to 13/06–18). The three perturbations all have pronounced influences on the cyclone, depending on their magnitudes and position with respect to the cyclone center. At 12/12–00, Q_{d2} is located west of Q_{d1} and the two PV anomalies are separated by more than 3000 km (not shown). Therefore, the interactions between Q_{d1} and Q_{d2} are weak and the background flow dominates the evolution, acting to advect Q_{d1} southeastward and Q_{d2} eastward.

Because the 400-hPa background flow is slightly diffluent downstream of the Rocky Mountains, northerly flows behind the trough axis decrease southward in intensity. This flow structure tends to advect Q_{d1} faster than Q_{d2} toward the cyclone center. The approaching of the two positive PV anomalies coincides with the rapid intensification of the system (Huo et al. 1995; Kocin et al. 1995). On the other hand, the R-induced flow, which is diffluent northwestward, assists further the merging of Q_{d1} and Q_{d2}, but slows their eastward movements. The net result is that by 12/18–06, the two anomalies are brought together within a distance of less than 2000 km (Fig. 8a); so the vortex–vortex interactions become significant. Clearly, the Q_{d2}-induced circulation tends to force Q_{d1} to move westward away from the genesis area while enhancing the moisture transport and the vorticity advection toward the cyclone center. Similarly, the Q_{d1}-induced circulation tends to advect Q_{d2} and a colder air mass toward the

genesis area. Because of the complicated interaction, it is not possible to determine the relative integral effects of Q_{d1} and Q_{d2} on the cyclogenesis. Their individual influences could only be examined by treating Q_{d1} and Q_{d2} separately as an initial-value problem. This will be discussed in Part II (Huo et al. 1999).

By 13/06–18 (Fig. 8b), the two positive PV anomalies are being advected farther toward the surface cyclone and the system begins to reach its most rapid deepening stage. Of interest is that both the R- and the Q_{d1}-induced circulations increase, owing to the mid-level rapid latent heat release along the warm front and the continued descending of stratospheric air behind the trough axis. However, the Q_{d2}-induced circulation weakens from -20 to -16 dam during the prior 12 h. As shown in Fig. 1, Q_{d1} continues to intensify as it moves southeastward whereas Q_{d2} weakens as it moves northeastward, causing changes in the orientation of the upper-level troughs. The weakening of Q_{d2} and strengthening of Q_{d1} can be understood as the interaction of background PV with the Q_{d1}- and Q_{d2}-induced circulations. Specifically, the Q_{d1}- (Q_{d2}-) induced winds are southerly (northerly) at Q_{d2} (Q_{d1}), thus weakening Q_{d2} (strengthening Q_{d1}) by advecting background PV. In the height field, this is the time when the two upper-level troughs start to merge together and produce a negative meridional tilt of the trough axis. Thus, the transition of the trough axis from the positive to negative tilt, a characteristic of the trough-merger climatology (Gaza and Bosart 1990), may be a manifestation of the interaction between the two upper-level positive anomalies.

To quantify the relative importance of these different interactions in the anomaly development and surface cyclogenesis, we calculate the instantaneous PV tendencies induced by each of the above-mentioned advective processes. The results for 13/00–12 are given in Fig. 9, which supports the conceptual model given in Fig. 7 but shows significantly varying magnitudes and structures of individual anomalies. For example, the Q_{d1}-induced flow advects the background PV to create a positive (negative) PV tendency to its west (east), acting to propagate itself westward (Fig. 9a). For the same reason, the Q_{d2}-induced flow also acts to propagate itself westward, but much weaker than Q_{d1} (Fig. 9b). The advection of the background PV by the R-induced anticyclonic circulation is more complicated (see Fig. 9c) due to the presence of local maxima in the background PV field (e.g., south of the Great Lakes and off the coast of Nova Scotia; see Fig. 8). On average, the R-induced flow causes PV increases (or height falls) to its east and PV decreases (or height rises) to its west.

Figures 9d–f show the tendencies due to each of the Q_{d1}-, Q_{d2}-, R-induced flows advecting the other two PV anomalies. Although these tendencies are localized, the magnitudes are much larger than those self-propagation terms as shown in Figs. 9a–c (note the different

contour intervals between Figs. 9a–c and 9d–h). We see that the Q_{d1}-induced flow forces Q_{d2} to move eastward and R to move northward (Fig. 9d), which is consistent with the results obtained from the static PV inversion (Fig. 8b). Similarly, the Q_{d2}-induced flow acts to move R northwestward and Q_{d1} westward against the background flow (Fig. 9e). Like the case in Fig. 7b, the R-induced flow tends to advect both Q_{d1} and Q_{d2} northward.

The more pronounced dynamic forcing is associated with the advection by the background flow, which acts to advect all the PV anomalies downstream: Q_{d1} southeastward and Q_{d2} eastward, both toward the surface cyclone (Fig. 9g). This results in a broad area of positive PV tendency between positive (Q_{d1} and Q_{d2}) and negative (R) anomalies. More importantly, this large area of positive PV tendency coincides closely with the surface cyclogenesis area, and its magnitude dominates all the vortex–vortex interactions. Therefore, the sum of all the elements yields the total PV tendency (Fig. 9h), which is dominated by background advection and modulated by the vortex interactions.

Based on the above analysis, it is evident that in the absence of both Q_{d1} and Q_{d2} (or the upper-level short-wave troughs) the surface cyclogenesis could not take place, at least during the 36-h integration period despite the presence of intense baroclinicity. What would happen to the surface cyclogenesis in the case of only having Q_{d1} or Q_{d2}? Based on the above discussion, we may infer that without Q_{d1}, the advection of Q_{d2} toward the cyclogenesis area would be reduced due to the decreased eastward component of the flow associated with Q_{d1}. Thus, the eastward movement of the surface cyclone (if developed) would be slow. Without Q_{d2}, the background flow would tend to advect Q_{d1} faster toward the surface cyclone for its deepening. These hypotheses will be tested in Part II of this series of papers through a series of sensitivity experiments (see Huo et al. 1999).

Finally, let us examine the formation of the upper-level jet streak (Fig. 1) in the context of the PV concept since its transverse circulations have been indicated by Huo et al. (1995) and Kocin et al. (1995) to play an important role in the rapid development of the storm. Here we may visualize the upper-level outflow jet streak as the superposition of circulations associated with Q_{d1}, Q_{d2}, R, and background PV as given in Fig. 8. Two vertical cross sections of the inverted height normal to the jet streak are taken to see their relative contributions: one near the entrance region (Figs. 10a–d) and the other near the R-induced circulation center (Figs. 10e–h). In the entrance region, the Q_{d1}, R, and background PV-induced circulations contribute approximately equally to the upper-level jet streak (i.e., the winds in the jet core region); Q_{d2}'s contribution is slightly negative and negligible. In the core region, only the R-induced and background flows are important whereas Q_{d1} and Q_{d2}'s contribu-
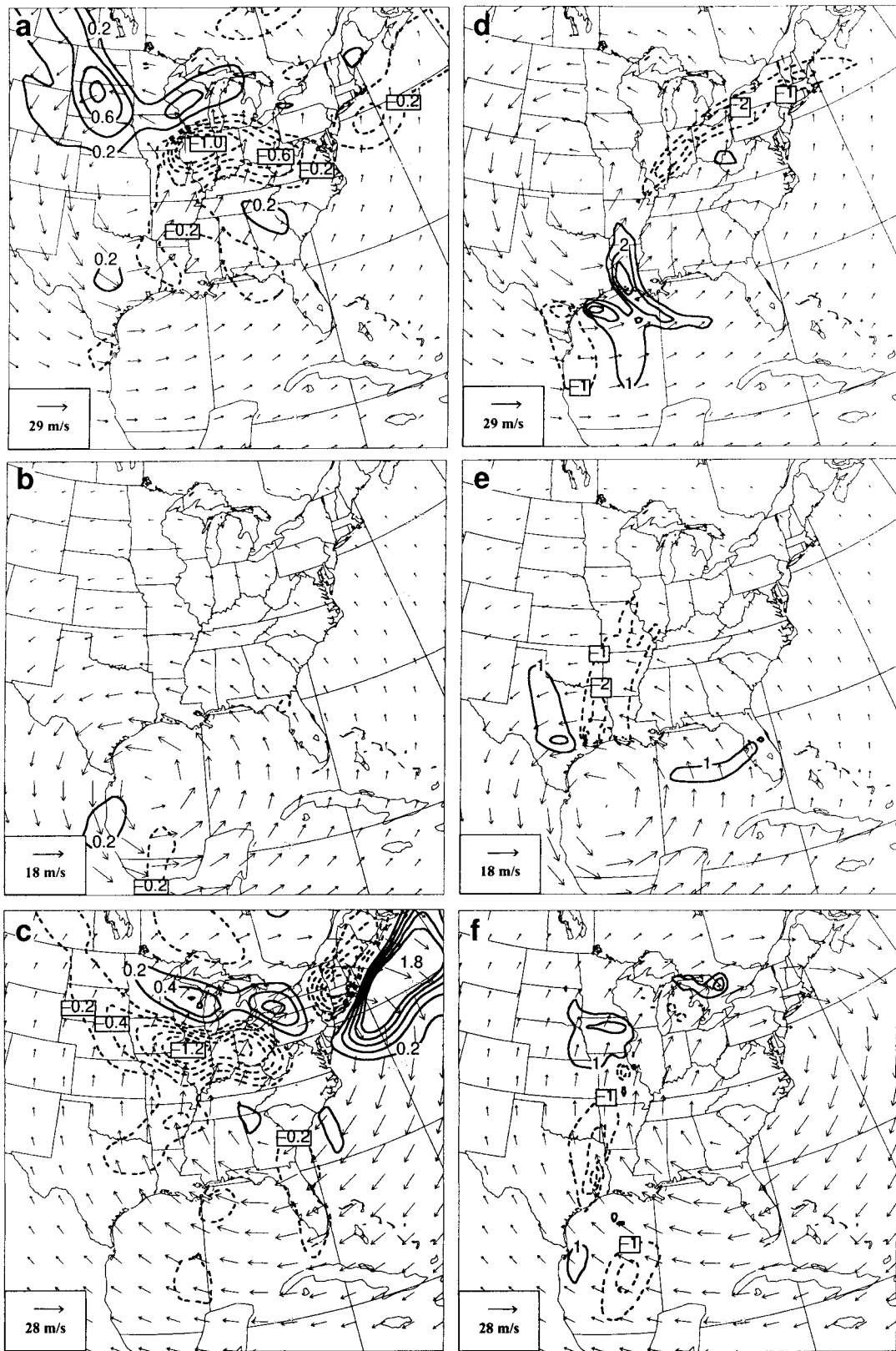
FIG. 9. The PV advection at 13/00–12 by the balanced flows that are inverted from (a) Q_{d1}, (b) Q_{d2}, and (c) R advecting the background PV; (d) the northern PV anomaly Q_{d1}, (e) the southern PV anomaly Q_{d2}, (f) the negative PV anomaly R advecting the other two PV anomalies;
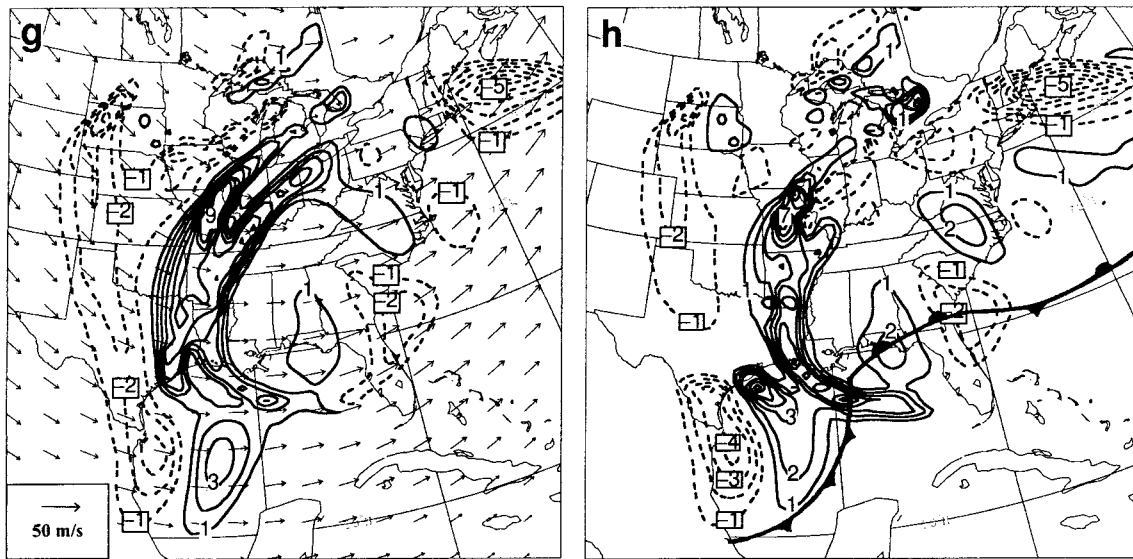
FIG. 9. (*Continued*) (g) background flow advecting Q_{d1}, Q_{d2}, and *R*. The total tendency is given in (h). Note that the contour intervals for (a)–(c) are 0.2 PVU/6 h, and 1 PVU/6 h for (d)–(h). Solid (dashed) lines are for positive (negative) values.

tions are negligible. Without the PV perturbations, the large-scale jet stream could still exist (see Figs. 10d,h) due to the presence of the large-scale baroclinicity. However, the *R*-induced circulation plays an important role in the formation of the outflow jet streak (Figs. 10c,g). Throughout the development period, there is a significant increase of *R* and its associated circulation, and consequently the outflow jet. As discussed earlier, the increase of *R* is closely related to the latent heat release along the warm front and near the cyclone center, aided by the transport of moisture through the jet-streak-induced transverse circulation (Huo et al. 1995). Thus, we may state that the intensification of the upper-level jet streak results from a positive feedback among latent heating, moisture transport, and transverse circulation.

7. Summary and conclusions

The contributions of various potential vorticity perturbations to and their mutual interactions on the superstorm of 12–14 March 1993 are investigated by using a piecewise PV inversion diagnostic system. This study is aimed at the vertical and lateral interactions among various distinct PV anomalies: upper-level dry positive PV anomalies consisting of a northern and a southern PV anomaly, the upper-level negative PV anomaly, the lower-level moist PV anomaly, and the surface thermal anomalies. It is shown that the absolute contributions (to the surface cyclone depth) from the above anomalies increase with time, but their relative importance varies during the genesis stages. At the mature stage, the upper-level dry PV anomaly contributes the most to the surface cyclone depth (53%),

followed by the surface thermal anomaly or thermal advection (28%). The low- to midlevel moist PV anomaly contributes the least (19%) to the genesis, and its relative significance remains nearly unchanged during the life cycle of the storm.

By comparing the PV anomalies and their inverted circulations, we found that there exists a favorable phase tilt between the upper- and lower-level anomalies that allows lower-level–upper-level mutual interactions. That is, the circulations associated with the upper-level PV anomalies enhance the lower-level anomalies, which in turn feedback positively to the upper-level perturbations. In addition to the vertical interactions, lateral interactions are also present among the upper-level PV anomalies and the background flow. It is found that the background flow advection dominates the vortex–vortex and vortex–background flow interactions. The vortex–vortex interaction of the two upper-level positive PV anomalies (or two troughs) causes the negative tilt of the main upper-level trough during the rapid deepening stage. The negative PV anomaly associated with an upper-level ridge plays an important role in the formation of the upper-level outflow jet. To isolate the impacts of the upper-level troughs and their interaction with diabatic heating and large-scale baroclinicity on the cyclogenesis, we have to find a way to separate these perturbations first in the model initial conditions and then evaluate their impacts by treating them as an initial value problem. This will be presented in Part II of this series of papers through the analysis of various sensitivity experiments to the above-mentioned PV perturbations.
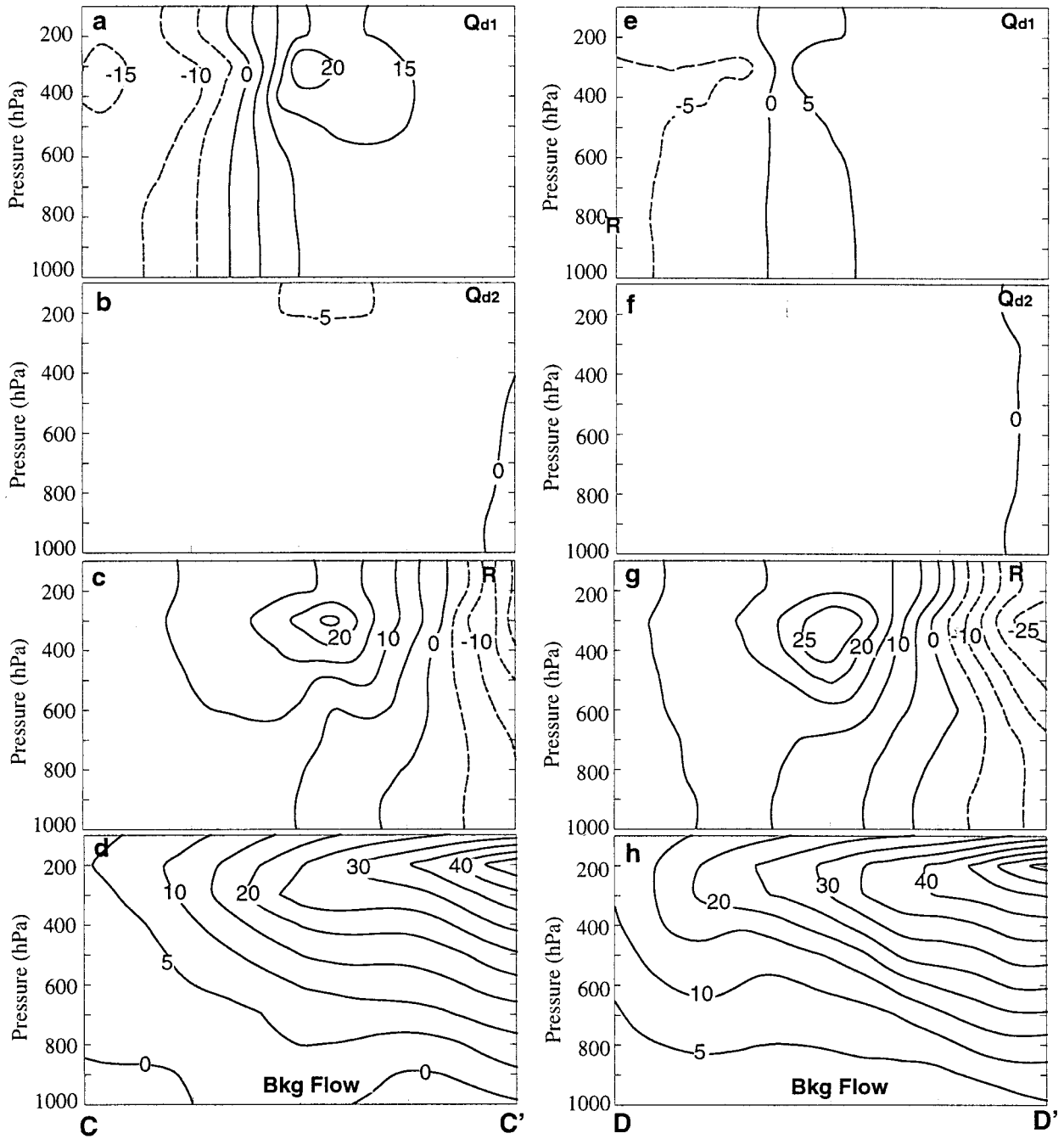
FIG. 10. Vertical cross sections of section-normal wind speeds (m s^{-1}, positive into and negative out of the page) that are inverted from (a) and (e) Q_{d1}, (b) and (f) Q_{d2}, (c) and (g) R, (d) and (h) background flow, which are taken along lines CC' and DD' as shown in Fig. 1b.

REFERENCES

Black, R. X., and R. M. Dole, 1993: The dynamics of large-scale cyclogenesis over the North Pacific Ocean. *J. Atmos. Sci.,* **50,** 421–442.

Bleck, R., 1990: Depiction of upper/lower vortex interaction associated with extratropical cyclogenesis. *Mon. Wea. Rev.,* **118,** 573–585.

Boyle, J. S., and L. F. Bosart, 1986: Cyclone-anticyclone couplets over North America. Part II: Analysis of a major cyclone event over the eastern United States. *Mon. Wea. Rev.,* **114,** 2432–2465.

Davis, C. A., 1992: A potential-vorticity diagnosis of the importance of initial structure and condensational heating in observed extratropical cyclogenesis. *Mon. Wea. Rev.,* **120,** 2409–2428.

——, and K. A. Emanuel, 1991: Potential vorticity diagnostics of cyclogenesis. *Mon. Wea. Rev.,* **119,** 1929–1953.

——, M. T. Stoelinga, and Y.-H. Kuo, 1993: The integrated effect of condensation in numerical simulation of extratropical cyclogenesis. *Mon. Wea. Rev.,* **121,** 2309–2330.

Gaza, R. S., and L. F. Bosart, 1990: Trough-merger characteristics over North America. *Wea. Forecasting,* **5,** 314–331.

Hakim, G. J., D. Keyser, and L. F. Bosart, 1996: The Ohio Valley wave-merger cyclogenesis event of 25–26 January 1978. Part II: Diagnosis using quasigeostrophic potential vorticity inversion. *Mon. Wea. Rev.,* **124,** 2176–2205.

Hoskins, B. J., M. E. McIntyre, and R. W. Robertson, 1985: On the use and significance of isentropic potential vorticity amps. *Quart. J. Roy. Meteor. Soc.,* **111,** 877–946.

Huo, Z., D.-L. Zhang, J. R. Gyakum, and A. N. Staniforth, 1995: A diagnostic analysis of the superstorm of March 1993. *Mon. Wea. Rev.,* **123,** 1740–1761.

——, ——, and ——, 1998: An application of potential vorticity inversion to improving the numerical prediction of the March 1993 superstorm. *Mon. Wea. Rev.,* **126,** 424–436.

——, ——, and ——, 1999: Interaction of potential vorticity anomalies in extratropical cyclogenesis. Part II: Sensitivity to initial perturbations. *Mon. Wea. Rev.,* **127,** 2563–2575.

Kocin, P. J., P. N. Schumacher, R. F. Morales, and L. W. Uccellini, 1995: Overview of the 12–14 March 1993 superstorm. *Bull. Amer. Meteor. Soc.,* **76,** 165–182.

Nielsen-Gammon, J. W., and R. J. Lefevre, 1996: Piecewise tendency diagnosis of dynamical processes governing the development of an upper-tropospheric mobile trough. *J. Atmos. Sci.,* **53,** 3120–3142.

Petterssen, S., 1956: *Weather Analysis and Forecasting.* 2d ed. Vol.1, *Motion and Motion Systems,* McGraw-Hill, 428 pp.

Reed, R. J., M. T. Stoelinga, and Y.-H. Kuo, 1992: A model-aided study of the origin and evolution of the anomalously high potential vorticity in the inner region of a rapidly deepening marine cyclone. *Mon. Wea. Rev.,* **120,** 893–913.

Sanders, F., 1986: Explosive cyclogenesis in the west-central North Atlantic Ocean, 1981–84. Part I: Composite structure and mean behavior. *Mon. Wea. Rev.,* **114,** 1781–1794.

——, 1988: Life histories of mobile troughs in the upper westerlies. *Mon. Wea. Rev.,* **116,** 2629–2648.

Uccellini, L. W., R. A. Petersen, K. F. Brill, P. Kocin, and J. J. Tuccillo, 1987: Synergistic interactions between an upper-level jet streak and diabatic processes that influence the development of a low-level jet and a secondary coastal cyclone. *Mon. Wea. Rev.,* **115,** 2227–2261.

——, P. J. Kocin, R. S. Schneider, P. M. Stokles, and R. A. Dorr, 1995: Forecasting the superstorm of 12–14 March 1993. *Bull. Amer. Meteor. Soc.,* **76,** 183–199.

Whitaker, J. S, L. W. Uccellini, and K. F. Brill, 1988: A model-based diagnostic study of the rapid development phase of the Presidents' Day cyclone. *Mon. Wea. Rev.,* **116,** 2337–2365.